Mohammed Faouzi Fekaouni[1,2], Patrick Maspeyrot[2], M. Hadj Meliani[3], Abdelkader Youcefi[1]

PASSIVE STRUCTURAL CONTROL OF A MODEL CAR DRAG BY TRANSVERSE SEPARATING PLATES

PASIVNO UPRAVLJANJE OTPORA MODELA KONSTRUKCIJE VOZILA PRIMENOM POPREČNIH RAZDVOJENIH PLOČA

Originalni naučni rad / Original scientific paper
UDK /UDC: 629.3.015

Rad primljen / Paper received: 5.03.2019

Adresa autora / Author's address:
1) Laboratoire ASP, Université des Sciences et de la Technologie d'Oran USTO, Oran, Algérie
email: fekaouni_mf@yahoo.fr
2) Institut P Prime UPR 3346 CNRS Université de Poitiers ISAE-ENSMA SP2MI -Téléport 2- Futuroscope Chasseneuil Cedex, France
3) Laboratory for Theoretical Physics and Material Physics, LPTPM, Department of Mechanics, Faculty of Science, Hassiba Benbouali University of Chlef, Algeria

Keywords
- automotive
- aerodynamic
- Ahmed body
- passive structural control
- flow control

Abstract

Reduction of aerodynamic drag is essential in optimizing the energy used regardless of its source and consequently to reduce emissions of pollutants. Passive structural control is simple to implement without additional energy, and it ensures the absence of electronic or sophisticated actuator. In this area very little research has been investigated and little work is done compared to active control. Among the techniques for passive structural control, shape optimization includes the addition of Transverse Separating Plates (TSP) soldered to the reduced model, positioned at the rear and arranged perpendicularly to the incident flow. The aim is to undertake a series of simulations on a reduced and simplified vehicle model (Ahmed body) placed in a channel by imposing a uniform speed of V_0 = 40 m/s and a Reynolds number of $Re = 2.75 \cdot 10^6$ and rear window angles of 15°, 35° and 90°. TSPs soldered to the body are positioned at the rear and arranged perpendicular to the direction of flow. We altered the plate dimensions (width and height), the different distances connecting the plate to the body, we successively analysed the size and distance of the TSP in order to optimize the embarked energy.

Ključne reči
- auto konstrukcije
- aerodinamika
- Ahmed telo
- pasivno upravljanje konstrukcija
- upravljanje strujanja

Izvod

Smanjenje aerodinamičkog otpora je veoma značajno u optimizaciji potrošnje energije, nezavisno od izvora, kao i za smanjenje emisije zagađivača. Pasivno upravljanje konstrukcijom, koja se jednostavno implementira bez dodatnog utroška energije, čini nepotrebnim ugradnju elektronskog ili sofisticiranog aktuatora. U ovoj oblasti je obavljeno vrlo malo istraživanja u poređenju sa aktivnim upravljanjem. Od tehnika za pasivnu kontrolu konstrukcije, optimizacija oblika podrazumeva dodatne poprečne razdvojene ploče (TSP) koje se spajaju lemljenjem za umanjeni model, postavljene na zadnji deo, normalno na pravac strujanja. Cilj rada je izvođenje serije simulacija na umanjenom i pojednostavljenom modelu vozila (Ahmed telo) postavljenim u kanalu sa uniformnom brzinom strujanja V_0 = 40 m/s i Rejnoldsovim brojem $Re = 2{,}75 \cdot 10^6$ i sa nagibima zadnjeg stakla od 15°, 35° i 90°. Elementi TSP, zalemljeni za telo, postavljeni su na zadnjem delu i orijentisani normalno na pravac strujanja. Izmenili smo dimenzije (širinu i visinu) ploče, različita rastojanja na mestima veze ploča za telo, i uspešno smo analizirali dimenzije i rastojanje TSP u cilju optimizacije utroška energije.

INTRODUCTION

Vehicle drag plays a crucial role in its performance relative to power losses that cause excessive fuel consumption and emissions of CO_2 /1/. It is shown that the drag force is about 80% of the total resistance of a medium-sized vehicle moving at a speed of 100 km/h (62 mph), /2, 3/. The intensity of the drag force is related to the drag coefficient (C_x) of the aerodynamic profile of the vehicle. The best profile is one that provides a laminar flow without separation of the boundary layer so that there is no turbulence at the rear of the vehicle. Recently, cars are increasingly being developed with ‘truncated’ areas constituted by an angled bezel, the right base, but in this work, the airflow detaches from the normal path and causes turbulence, which is responsible for 20% of the resistance to forward movement when the vehicle exceeds a certain speed threshold, /3/.

Studies show that the reduction in drag is done by a control solution that takes account of the performance of the geometry of the car and the flow around the car by use of external control systems, /2/. The performance of the real geometry is achieved by the Ahmed body /4/, which uses a simplified geometry, reduced to the scale 1:5 by following the studies of Janssen and Morel on a similar body that reproduces the actual flow around the vehicle as closely as possible /5, 6/. The second part of the solution is the use of the external control system, based on the control principle of the reattachment of the boundary layer to the wall. The two techniques are used to reduce drag: passive and active flow control, /3/. The method of passive flow control is obtained without an external power supply while the active control technique requires the input of external energy to the drag control system, /3/. There are many works on the active control of drag reduction and they mostly use jets that make it possible to dynamically reattach the recirculation on the bezel and to eliminate, reduce, or symmetrize the vortex structure supported on the base, /7, 8/. Passive control techniques include optimization of shape (base plate), vortex generators, surface state change, change in the local distribution of the parietal static pressures, self-adaptive surfaces, porous surface, and so on, while the active control techniques include mobile walls, continuous aspiration, continuous blowing, alternate blowing (pulsatile jets), alternating blowing and suction (synthetic jets), cold plasma, acoustic excitation, and so on. Passive control systems take the form of more or less discrete appendages that are added to the vehicle. According to Kourta and Gilliéron, these solutions can be described in two groups prioritized according to their control mechanism types, /1/. The barrier can be placed in \the vicinity of an upstream separation point to ensure a transfer of energy from the main flow toward the near-wall boundary layer in order to repel the detachment. It can also be used for the profile geometry and to avoid the formation of vortex structures, generally on the rear part of the vehicle. Altaf et al. /3/ suggest the following classification into three categories: (a) adding an element of reduction such as the separating plates; (b) control of surfaces like ribs and porous surface; and (c) changes such as cavities. Very little research has been done on the use of separation plates, and few works are known in this field. Gilieron and Kourta use a wind tunnel to test the Ahmed body with the use of separating plates at the front and the rear of the vehicle from different angles, /9-11/. Levallois et al. carried out experiments in a wind tunnel on a geometry representing the Ahmed body with a right cheek at a flow rate of 30 m/s and showed that transverse dividing plates can be used to tighten the near wake by 10% and obtain savings of about 11.6% drag, /12/. The plate used is placed at $0.7H$ downstream of the nerve, where H represents the height of the nerve. The section of the plate is $0.9H \times 0.85l$, where l is the width of the geometry.

The results indicate a strong correlation between the value of drag and the presence at the nerve of a stable vortex ring structure, that is, a structure whose vortex centres appear clearly. The flow is stuck back together to the periphery of the separator element level (points A and B, Fig. 1a). The flow takes afterwards a classic configuration right base type, with a classic configuration of the vortex structure based on the edge of the plate. The cross-section of wake S_2 is then less than the S_1 section obtained without control. The recirculation of the fluid in the cavity D (Fig. 1a) causes an increase in pressure at the level of the nerve to the geometry.

Figure 1b shows the distribution of pressure up to the level of the nerve in a median longitudinal plane. These results indicate that the presence of the plate tends to standardize and increase the pressure.

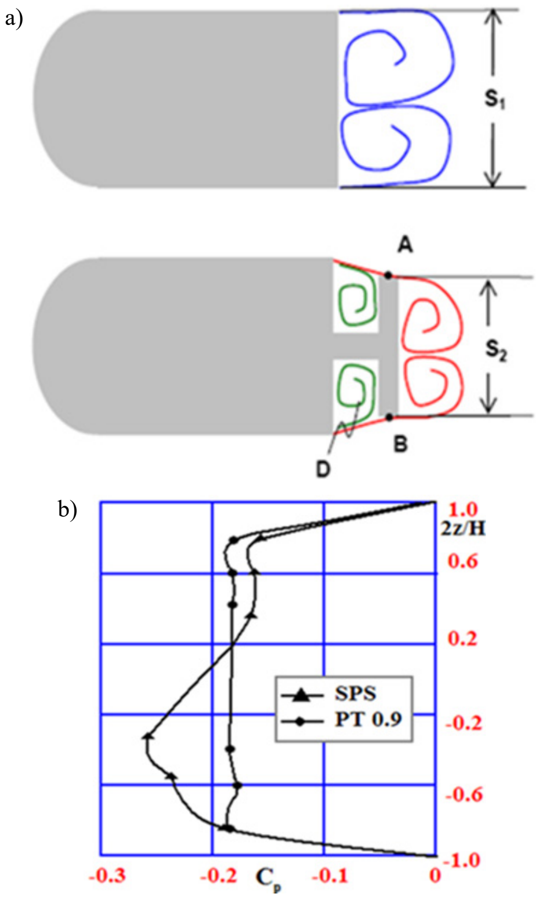

Figure 1. (a) TSP. The recirculation of fluid in cavity D causes an increase in pressure at the level of the base of origin. (b) Presence of the plate standardizes and increases the pressure, /12/.

The goal of our work is to undertake a series of simulations on a reduced and simplified vehicle model (Ahmed body) with rear window angles of 15, 35, and 90° placed in a channel. TSPs soldered to the body are positioned at the rear and arranged perpendicular to the direction of flow. By varying the dimensions (width and height) of the plate and the different distances connecting the plate to the body, we analyse successively the size and remoteness of the PST in order to optimise the energy used.

DESCRIPTION OF THE MODEL

The calculation for this study is a digital vein, which is a tunnel of cycle open or closed, where the Ahmed body is placed inside the vein, and air is introduced at the entrance of the vein (Fig. 2).

Ahmed body with Transversal Separator Plate (TSP)

The geometric dimensions selected for these simulations are those defined in Fig. 2. The length L, width l, and height H of the geometry are L = 1.044 m, l = 0.389 m, and H = 0.288 m. In this study, the rear window, with a length of

l_{la} = 0.222 m, is inclined at 25° to the horizontal, that is, the bottom of the basement, and is positioned at a height h = 0.05 m from the floor of the digital vein, /4, 12/. A PST solidarity to the body is positioned at the rear and arranged perpendicular to the direction of flow (Fig. 2). By varying the width (l_1) and height (h) of the plate and the distance (equal to M at the height of the rear base) from the plate to the body, where the width $l_1 = l = 0.389$ m, height $h_1 = H = 0.288$ m, and distance $M = H - l_{la}\sin\varphi$, with l_{la} = 0.222 m and φ respectively zero (right), 15 to 35°.

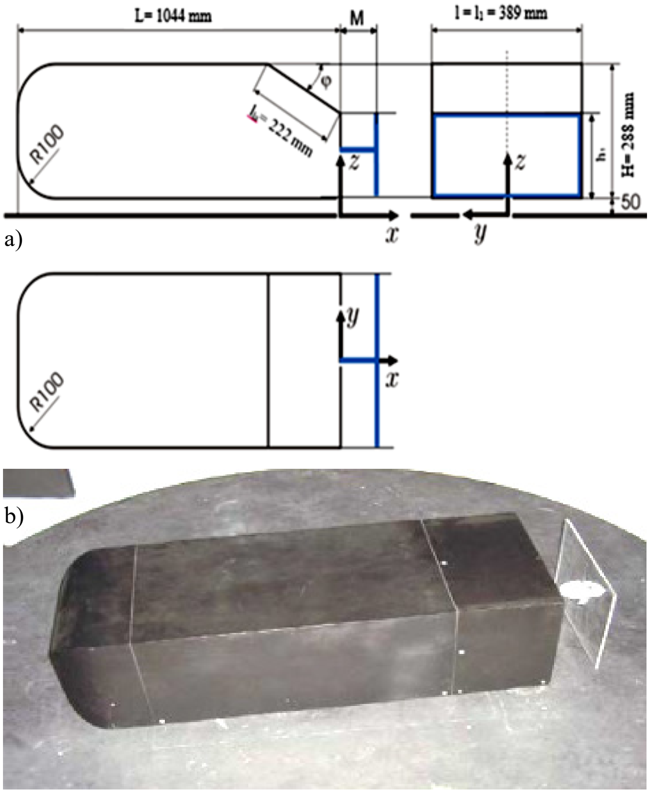

Figure 2. (a) Ahmed body dimensions and available to the TSP /4, 12, 13/; (b) PST arranged downstream of the Ahmed body for a right base, /12/.

Tunnel and operating conditions

The geometry is placed in a square channel whose width l_1 and height H_1 are equal to $2L$, and whose length L_1 equals eight times the length of the obstacle (L = 1044 mm). The geometry is located at a distance of $2L$ from the entrance to the channel, /14/. These important dimensions make it possible to avoid possible interactions between the conditions imposed on the flow to the limits of the field of simulation and main flow (in the vicinity of the geometry) and, in particular, to avoid any rise in pressure. The exit condition, that is, the downstream (output) geometry and geometry of the upper part (ceiling), allows the air to flow freely. Given the distance left to the back of the geometry, a static pressure condition is imposed. The pressure on the exit surface is uniform and has a value of P_0 = 101325 Pa. The condition of entry, applied on the face on the left side of the field of simulation (input), imposes a uniform speed of V_0 = 40 m/s and a Reynolds number, reduced to the length of the geometry, of Re = 2.75×10^6 (Fig. 3).

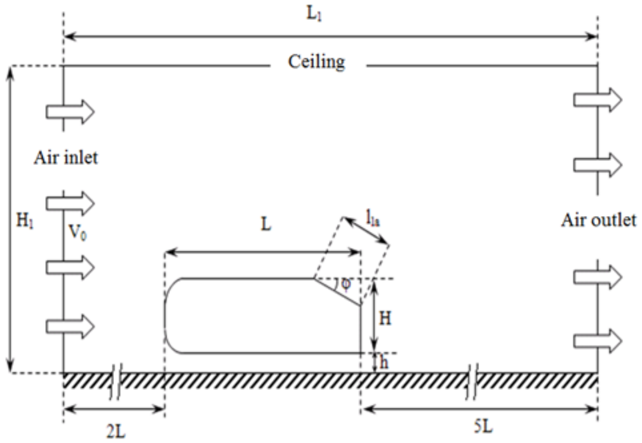

Figure 3. Implementation of the Ahmed body in the tunnel.

BASIC EQUATIONS AND BACKGROUND

The effort exerted by the flow on the geometry can be decomposed into an effort to drag F_x in the longitudinal direction, an effort to lift F_z according to the vertical direction, and an effort side F_y according to the transversal direction. The only drag is directly related to consumption. The expression of the trail is then given by the integral of the efforts of pressure, the tensor of viscosity, and the Reynolds tensor (the tensor of the efforts of turbulence) constraints on the geometry, considered according to the relation:

$$F_x = \left(\int_{S_c} \overline{\overline{Pl}}\,\vec{n}\,d\sigma - \int_{S_c} (\overline{\overline{\tau}}_\mu + \overline{\overline{\tau}}_t)\vec{n}\,d\sigma \right)\vec{x}\,, \qquad (1)$$

where: S_c represents the surface of the geometry; $\vec{n}$ is the vector outgoing normal to the surface S_c; $\overline{\overline{Pl}}$ is the tensor stress pressure; $\overline{\overline{\tau}}_t$ is the tensor from the constraints of turbulence; and $\overline{\overline{\tau}}_\mu$ is the tensor viscous stresses.

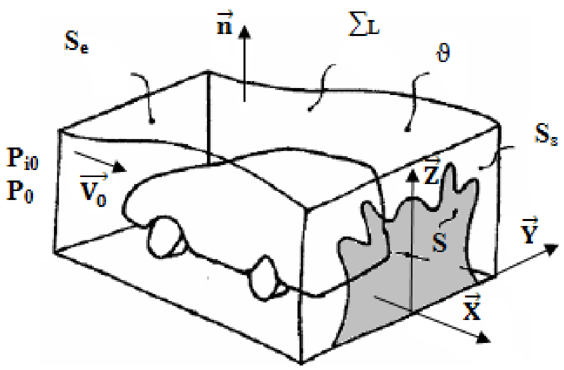

Figure 4. Full review of momentum, /20/.

The integration of constraints limited the surface border S_c of the body, to set the aerodynamic contact pressure and actions of viscous and turbulent origin applied to the vehicle. The aerodynamic actions of viscous and turbulent origin $\vec{F}_{\mu,t}$ are related to the formation of limits layers that develop on the surface of the border S_c. Aerodynamic pressure stocks $\vec{F}_p$ are functions of the geometry of the vehicle and resulting pressures associated with the external local detachments (mirror, amount of windshield) or internal (air that has entered) and pressures associated with the issued in the wake vortices. All these constraints are strongly related to each other. The result of aerodynamic actions of pressure is given by Eq.(1), which is expressed in terms of the static pressure coefficient C_p, defined by:

$$C_p = \frac{P-P_0}{\frac{\rho V_0^2}{2}}, \qquad (2)$$

$$\vec{F}_{px} = \frac{\rho}{2} V_0^2 \int_{S_c} C_p \vec{n}.\vec{x}\, d\sigma, \qquad (3)$$

where: P_0 is the static pressure; and $\vec{x}$ refers to the unit same sense and collinear vector to the vector speed V_0 of infinite flow upstream. For a rounded front without detachment of Rankine half-oval type, the aerodynamic drag is directly driven by the distribution of static pressure to the base. In general, and on a motor vehicle, the coefficients of static pressure C_p to the nerve are between -0.05 and -0.20. The objective of the flow control is to make the coefficients of static base pressure approach a value of zero. On a sedan-type motor vehicle, the aerodynamic pressure and friction stocks represent 90 and 10% of the total aerodynamic drag, respectively. Aerodynamic drag can also be analysed from the information distributed on the surface of the border, Σ_e, (Fig. 4) and contained mainly in the wake. In this case, its expression is given by:

$$F_x = \left[-\int_{\Sigma_e} (P-P_0)\bar{\bar{I}}\vec{n}\, d\sigma + \int_{\Sigma_e} (\bar{\bar{\tau}}_\mu - \bar{\bar{\tau}}_t)\vec{n}\, d\sigma \right].\vec{x} - \\ - \int_{\Sigma_e} \rho \vec{V}.\vec{x}\vec{V}.\vec{n}\, d\sigma \qquad (4)$$

For values averaged in the sense of turbulence and by choosing to not take into account the constraints of turbulent origin, this integral form can be expressed by the relationship given by Onorato et al.:

$$F_x = \underbrace{-\frac{\rho V_0^2}{2}\int_S \left(1-\frac{V_x}{V_0}\right)^2 d\sigma}_{(a)} + \underbrace{\frac{\rho V_0^2}{2}\int_S \left(\frac{V_y^2}{V_0^2}+\frac{V_z^2}{V_0^2}\right) d\sigma}_{(b)} + \\ + \underbrace{\int_S (P_{i0}-P_i)\, d\sigma}_{(c)}, \qquad (5)$$

where: P_{i0} represents the stop pressure of an infinite flow; upstream speed V_0; and P_i is the local stop pressure associated with the local speed $\vec{V}$ of components V_x, V_y, and V_z. The surface S is a section of measure located downstream of the base and transverse to V_0, Eq.(5). The aerodynamic drag is directly driven by the area S of the fluid field bounded by the outer contour of the wake in a cross-cutting plan in the direction of the cross-flow. The longitudinal component of the speed quickly approaches the speed of cross-flow and the first (a) integral of Eq.(5) tends towards zero, /7/. The second integral (b), the function of the kinetic energy of rotation calculated from transversal components V_y and V_z, translated the wake vortex trail. The last integral, (c) is calculated from pressure losses of downtime between the upstream and downstream of the vehicle, translates the drag associated with the formation and maintenance of wake vortex structures. Integrals (a), (b), and (c) are interrelated. The contributions of integrals (b) and (c) to the aerodynamic drag are close to 20 and 80 %, respectively. Aerodynamic drag reduction is then obtained by reducing the cross-sectional dimensions of the wake (cross-sectional area of integration S) and the number and development of the protruding vortex structures that originate in the proximity of the vehicles volume or cross-cutting speeds (in the y0z plane) longitudinal vortex structures. All of these structures are from the detachments, including the locations and positions are functions of the local curvature of the wall, the gradient of static pressure in the local direction of the flow, /16/, the rate of cross-flow turbulence /17/, or the roughness, /18/.

SIMULATIONS

Modelling of the boundary layer

A motor vehicle is a body of low elongation, with cavities and a nerve, that travels close to the ground, where local changes very quickly become an essential turbulent flow. The development of the boundary layer generates detachments that directly influence the structure of the flow in the wake and the value of the aerodynamic tensor exerted on the vehicle, /7/. In the boundary layer and especially in distant areas, the direction, sense, and norm of the vector of speed are changing rapidly, and modelling of the physical phenomena is still difficult to implement. This difficulty is related to the model used to represent the turbulence and on the other hand, the quality and the density of the mesh used to model the flow in the boundary layer of the wake. Turbulence models today are still inadequate to represent the complexity of three-dimensional flow around automobiles, and the quality and density of the mesh in the boundary layer must be considered as a prerequisite for their use. The solution is obtained from the Navier-Stokes equations averaged in the sense of turbulence. Each variable is then represented by an average component and a fluctuating component that describes the randomness of the flow from a coarser mesh and a very important time step. Averaged equations relate to the instantaneous equations but contain additional terms called forced, Reynolds. These constraints represent the effect of turbulent fluctuations on the mean flow. Air is introduced at atmospheric pressure (1 bar) and room temperature (25 °C) with a speed of 40 m/s and tolerances of 10^{-5} for the EDP. The comparison of the models used in the context of the complex flows in the industrial field, namely $k-\varepsilon$, $k\ \omega$, and $k-\ \omega$ SST, show that for different meshes (184322 and 369088), the model $k-\varepsilon$ is the fastest (728 seconds) with the smallest number of iterations (42) and without problems at the level of the EDP and convergence.

Effectively, the model $k-\ \varepsilon$ remains widely used; k refers to the turbulent kinetic energy mass (J/kg) and the rate of dissipation of this energy ε (W/kg). The model $k-\varepsilon$, however, does not represent the flow in the vicinity of the wall. The solution is to define specific templates that are valid only in the volume close to the wall. These models called laws of wall, replace the transport equations averaged in the sense of turbulence in the vicinity of the wall.

They represent a continuous evolution of the vector of speed in the boundary layer. As such, local continuity with the speed obtained by resolution of the Navier-Stokes equations averaged in the sense of turbulence is satisfied, /8/. The method of the fluid field in the turbulent boundary layer mesh generation is proposed to model the three-dimensional velocity field in the vicinity of the wall. The technique is to estimate the position of the detachment in the meaning of the cross-flow (v = 40 m/s) counted from the front of the vehicle, and to determine the local friction coefficient ($C_f = 3.07\cdot10^{-3}$) associated with the flow not off. This value is then used to determine the height of the first stitch ($y = 0.48\cdot10^{-3}$ m) from the number of Reynolds typical y^+ (between 30 and 50), /17/; $y^+ = 50$ is chosen with respect to the importance given to the restoration of the boundary layer) attached to the area of validity of the Law of the Wall. The use of this technique to model external flows around the Ahmed body makes it possible to restore the line in the vicinity of the wall friction and to represent a satisfactory evolution of vortex structures in the wake, /8/.

Mesh used

The structured mesh is shown longitudinal in Fig. 5a and is composed of 3516 nodes and 169322 mesh elements. This one was selected from several, since tests on finer meshes (containing 369088 mesh elements and 67635 nodes) revealed discrepancies relating to 5 % only on the variation of speed V on Y to the intersection of plane from wakes to 3.3 m from the entrance with surface symmetry, Fig. 5b. This mesh is a little more refined in the close wall of the Ahmed body (boundary layer).

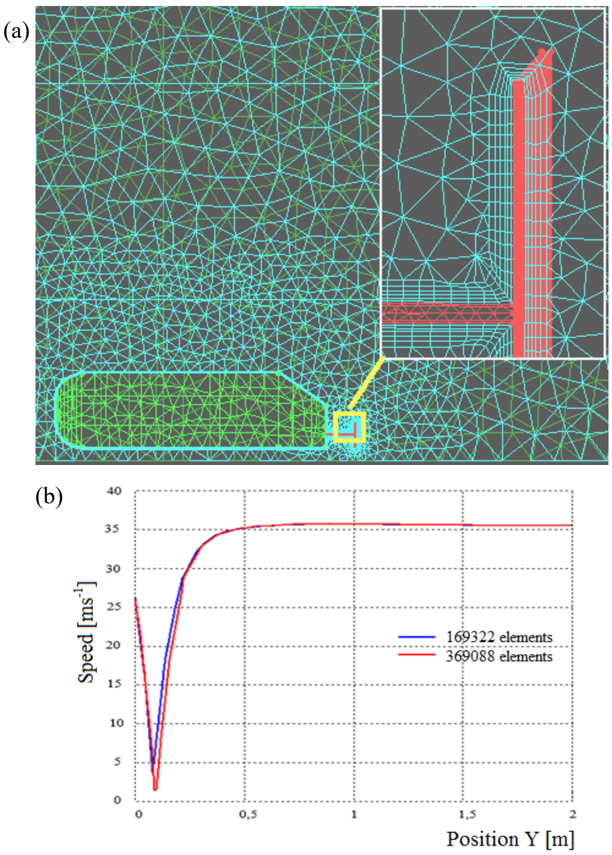

Figure 5. (a) Studied field mesh; (b) variation of speed V on Y.

Calculation domain

The calculation for this study is a digital vein, which is an open or closed tunnel, a cycle in which the Ahmed body is placed. We introduce air at the entrance of the vein. The pressure on the exit surface is uniform and has a value of P_0 = 101325 Pa. The condition of entry applied on the face on the left side of the field of simulation (input) imposes a uniform speed of V_0 = 40 m/s, that is, a Reynolds number of Re = $2.75\cdot10^6$, reduced to the length of the geometry, Fig. 6.

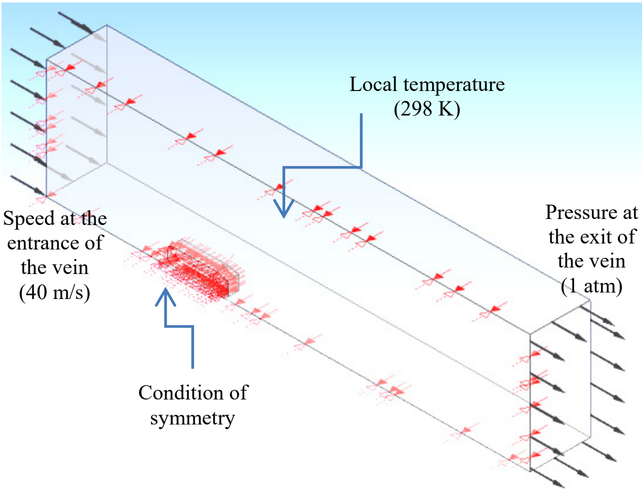

Figure 6. Implementation and simulation of boundary conditions.

Calculation code

We used the commercial code ANSYS CFX; (i) once the models have been chosen (type of equations in partial derivatives (EDP) to be solved), the operating conditions (air inlet, high wall, wall of floor, wall of the Ahmed body, output of air, and axis of symmetry) are fixed, and since the code work is by volumes method finished, the following information must be specified; (ii) diagram of pressure-speed coupling: the scheme to be adapted classic simplex; (iii) boundary values in these area conditions are directly assigned to the initial values. Maximum errors that must not be exceeded must be set, and for it to be adapted the tolerances are $\varepsilon = 10^{-5}$ to all EDP. The user imposes a maximum number of iterations for the simulation but if the residue in the calculations of the EDP is greater than the tolerances set by the user ($\varepsilon = 10^{-5}$), the simulation stops. The residue of the linear system is defined so that it is small enough for the code to perform 20 iterations consistently, maximum limit calculation code, with each iteration at the time also, no time is voluntarily taking much lower than the limit dictated by the stability of the code, which makes it possible to minimize the error made by the code at each iteration.

RESULTS AND DISCUSSION

We vary the height (h_1) and width (l_1) of the PST and the distance (M) from the TSP with the Ahmed body. The nominal values of h_1 and l_1 are equal to the height of the nerve back and the width of the Ahmed body, respectively, and the value of the distance M is equal to the height of the rear base of the Ahmed body. As the height of the rear base of the Ahmed body varies depending on the angle of the rear window (φ), $h_1 = M = H - l_{la}\cdot\sin\varphi$, with l_{la} = 0.222 m and φ equal to 0, 15 and 35°, respectively. After the choice of the unit height h_1 and l_1 of PST unit length and the distances of remoteness, h_1 and l_1 are varied in the same 0.9 reductions; 0.8 and 0.7; fixed l_1 is varied in h_1 for the reductions 0.9; 0.8 and 0.7 and then fixed h_1 is varied in l_1 for 0.9 reductions; 0.8 and 0.7. We repeat these simulations for distances of remoteness M of 1.0, 0.9, 0.8, and 0.7 and for angles of the rear window of 15°, 35°, and right.

The speeds noted in the vertical and horizontal planes for different relative positions of TSP are shown in Figs. 7, 9, and 11, respectively. The vertical plane to clearly highlight two vortex centres that appear and evolve is based on the relative distance of the separator element compared to the

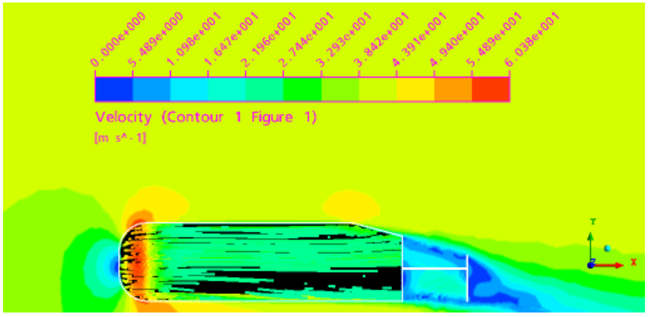

(a) $0.7h_1 – 0.7l_1$/distance M

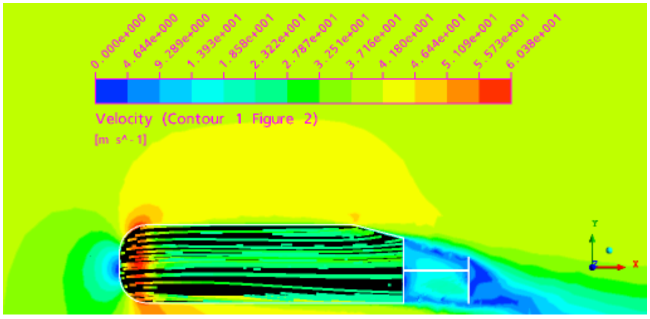

(b) $0.7h_1 – 0.9l_1$/distance M

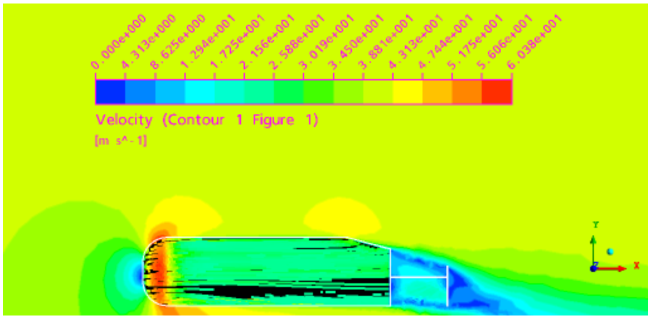

(c) $0.7h_1 – 0.9l_1$/distance M

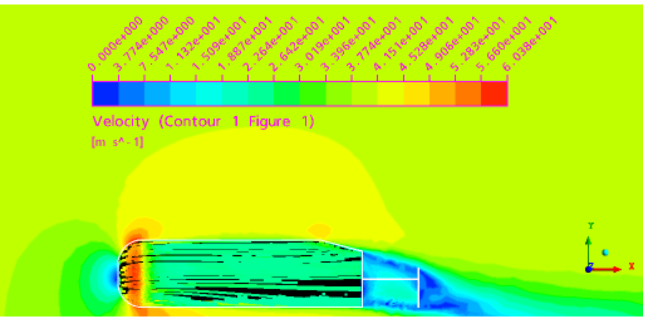

(d) $0.7h_1 – l_1$/distance M

Figure 7. Distributions of average speeds for a rear window at 15° with a PST of different dimensions and position of TSP at M.

nerve, /12/. When distance M increases, the vortex centres move downstream in the direction of TSP and maximum drag reduction is obtained when the vortex centres up and down are halfway up high and low hollows, and halfway between the base and the separator element, M_{CD} = 0.7M (see Fig. 11). Beyond this position, the upper vortex centre continues moving in the direction of cross-flow and approximates the separator element. The lower vortex centre moves to the ground and the PST. In all cases, the reduction of drag appears to be well associated with a reduction in the cross-section of the wake (surface S in Eq.(5)). For each dimension of TSP, the results show that an extreme exists and the best efficiency is obtained for special and distinct removals /12/, as verified in Figs. 8, 10, and 12. We vary h_1 and l_1 in the same reductions of 0.9, 0.8, and 0.7. Fixed l_1 and to vary h_1 for reductions 0.9; 0.8 and 0.7. Fixed h_1 and to vary l_1 for reductions 0.9; 0.8 and 0.7. We repeat these simulations for the removals M of 1.0, 0.9, 0.8, and 0.7. The authors note that for different rear window angles (15, 35 and 90°) and variation of distance M from TSP, the best drag coefficient is obtained for $0.7h_1 – 0.7l_1$; for distance of M reduced to 0.9, 0.8, and 0.7 we get almost the same value of the drag coefficient for remoteness, the C_x M(C_x) is significantly lower.

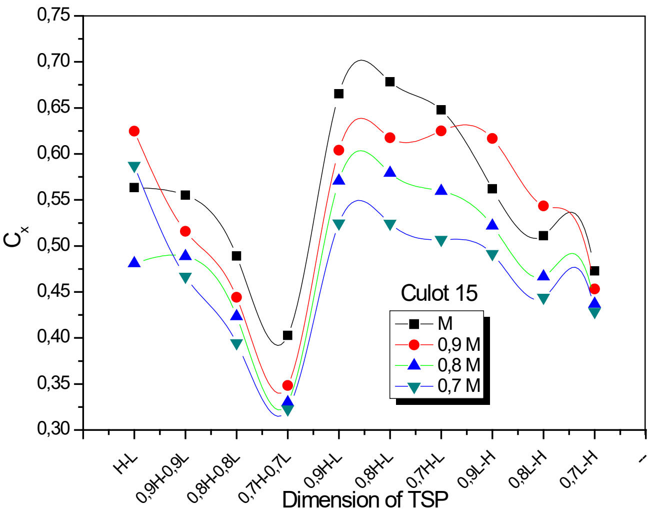

Figure 8. Drag C_x for rear window of 15° at different sizes and distances from TSP.

An increase in the trail is noted for TSP at $0.9h_1$ and l_1 and when you cut the drag, height decreases, similarly, an increased drag of lesser importance is noted for TSP of h_1 and l_1 and when the reduced drag length decreases. Generally, by setting h_1 and reducing l_1, we get the best C_x gain by setting l_1 and reducing h_1. The analysis shows that the positions of TSP that obtain maximum reduction of aerodynamic drag are not affected normally by the Reynolds number, and the aerodynamic drag decreases when the incident flow speed increases. This last result is according to classic automotive aerodynamics.

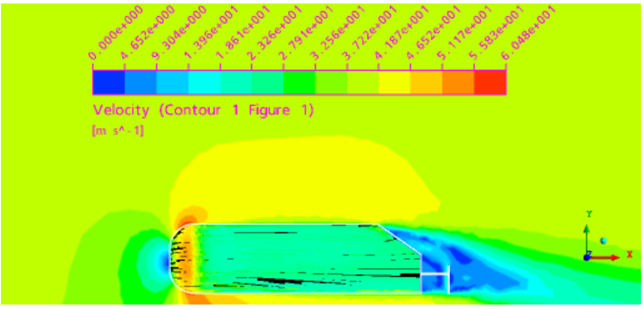

(a) $0.7h_1 - 0.7l_1$/distance 0.7M

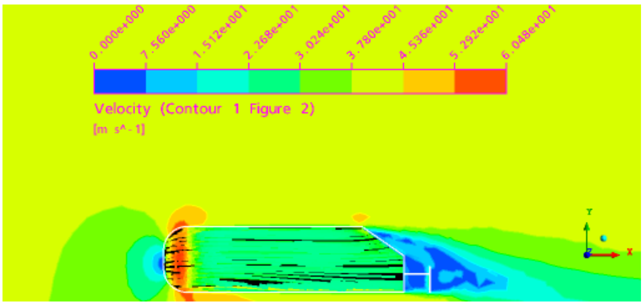

(c) $0.7h_1 - 0.9l_1$/distance 0.7M

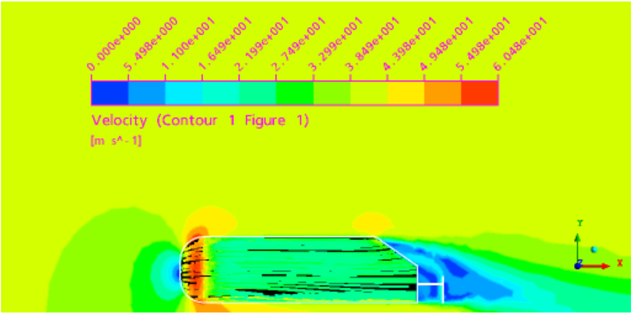

(b) $0.7h_1 - 0.8l_1$/distance 0.7M

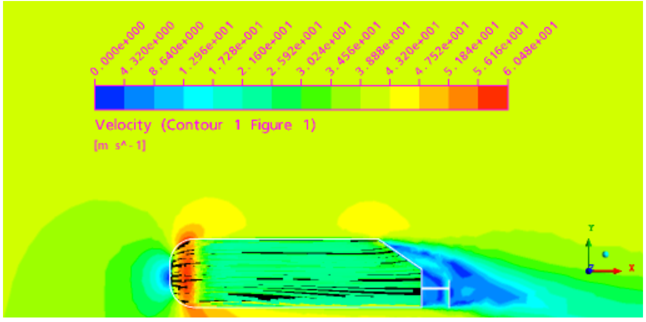

(d) $0.7h_1 - l_1$/distance 0.7M

Figure 9. Distributions of average speeds for rear window angle at 35° with PST of different dimensions and position of TSP at 0.7M.

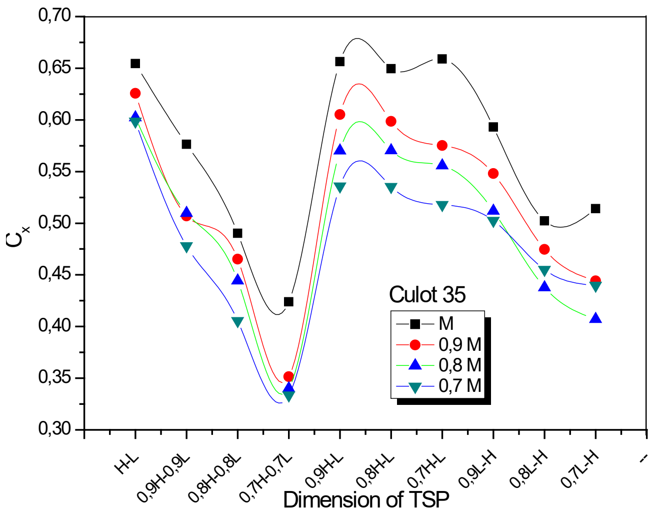

Figure 10. Drag C_x for rear window angle of 35° with different sizes and distances of TSP.

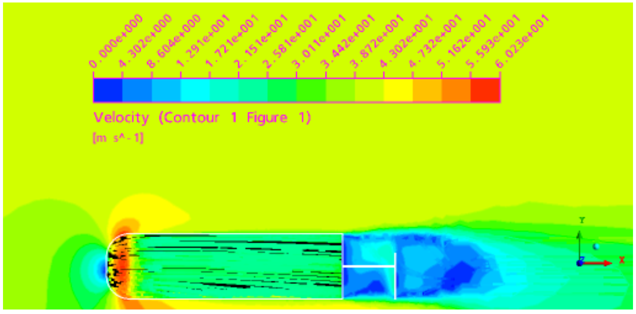

(b) $0.7h_1 - 0.7l_1$/distance 0.8M

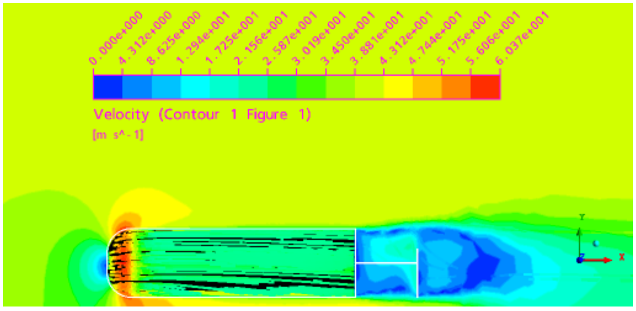

(c) $0.7h_1 - 0.7l_1$/distance 0.9M

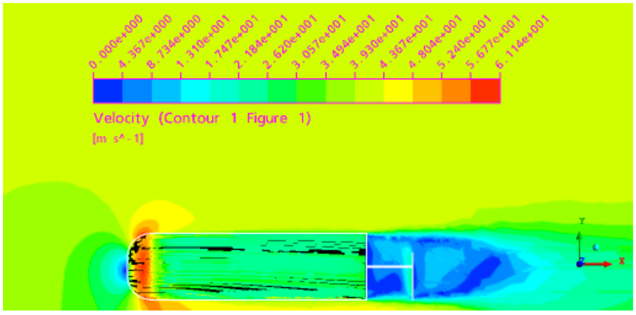

(a) $0.7h_1 - 0.7l_1$/distance 0.7M

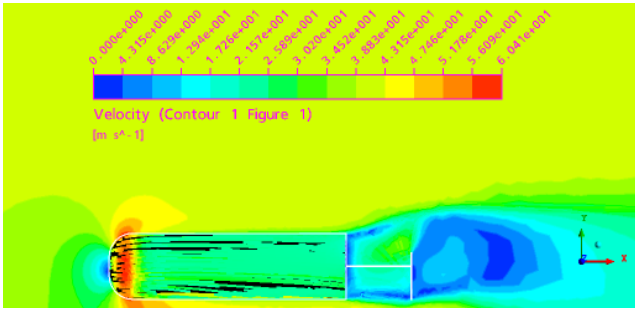

(d) $0.7h_1 - 0.7l_1$/distance M

Figure 11. Distributions of average speeds for rear window angle 90° with TSP at ($0.7h_1 - 0.7l_1$) and different positions of TSP (0.7M, 0.8M, 0.9M, and M).

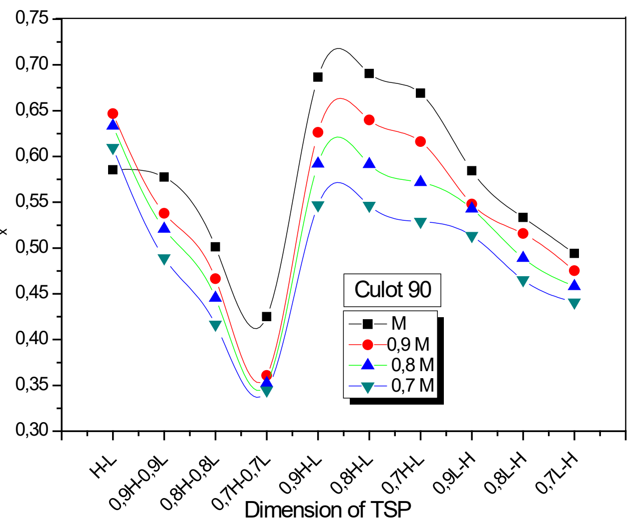

Figure 12. Drag *Cx* for a rear window angle of 90° with different size and distance of TSP.

CONCLUSION

The analysis shows positions of TSP required to obtain maximum reduction of aerodynamic drag. For three angles of the rear window at 15°, 35°, and right torque height/ width of the transverse separator plate, the best result is obtained for $h_1 0.7 – 0.7 l_1$ couple. The best distances for rear window angles of 15°, 30°, and 90° are 0.7M, 0.7M, and 0.8M, respectively. We can deduce that the distance to the Ahmed body standard is 0.7M for the three angles. Using a transverse separator plate, we get a loss of drag coefficient by 2.6% for the nerve 15°, and 3.1% for the nerve 35°, but a gain of 11.4% for the right base. The physical phenomena associated with this type of control are still little known.

Additional experiments are needed to determine such things as the re-examination of fluid at the level of points A and B. Such devices are potentially very interesting for the automotive industry. Significant reductions in drag are obtained for different units and particularly in the right nerve, can be roughly equated to a minivan-type vehicle or a commercial vehicle. However, many architectural problems related to the size of plate and aesthetics can delay the application of this type of solution. But it is of interest for exploitation in vehicles working trailers.

REFERENCES

1. Kourta, A., Guilliéron, P. (2009). *Impact of the automotive aerodynamic control on the economic issues*, J Appl. Fluid Mech. 2(2): 69-75.
2. Hucho, W.-H. (Ed.), Aerodynamics of Road Vehicles. From Fluid Mechanics to Vehicle Engineering, 1st ed., Butterworth-Heinemann, 1987.
3. Altaf, A., Omar, A.A., Asrar, W. (2014), *Review of passive drag reduction techniques for bluff road vehicles*, IIUM Eng. J 15(1): 61-69.
4. Ahmed, S.R., Ramm, G., Faitin, G. (1984), *Some salient features of the time-averaged ground vehicle wake*, SAE Tech. Paper 840300. doi: 10.4271/840300
5. Janssen, L.J., Hucho, W.-H. (1975), *Aerodynamische Formoptimierung der Typen VW Golf und VW Scirocco*, Automobiltechn. Z., 77:1-5
6. Morel, T. (1978), *Aerodynamic drag of bluff body shapes characteristic of hatch-back cars*, SAE Tech. Paper 780267. doi: 10.4271/780267
7. Leclerc, C. (2009). Réduction de la traînée d'un véhicule automobile simplifié à l'aide du contrôle actif par jet synthétique. Thèse de doctorat, Institut National Polytechnique de Toulouse
8. Baptista Peres, N., Pasquetti, R. (2013), *Étude numérique de la réduction de traînée d'un modèle d'un véhicule automobile par système de contrôle actif*, CFM 2013, 21ème Congrès Français de Mécanique, 2013, Bordeaux, France
9. Gilliéron, P., Kourta, A. (2010), *Aerodynamic drag reduction by vertical splitter plates*, Experiments in Fluids, 48 (1): 1-16. doi: 10.1007/s00348-009-0705-7
10. Kourta, A., Gilliéron, P. (2009). *Réduction de la trainée aérodynamique par plaques séparatrices verticales*, Revue de Mécanique Appliquée et Théorique, 2(1): 85-92.
11. Park, H., An, N.-H., Hutchins, N. et al. (2011), *Experimental investigation on the drag reducing efficiency of the outer-layer vertical blades*, J Marine Sci. Technol. 16(4): 390-401. doi: 10.1007/s00773-011-0135-0
12. Levallois, E., Gilliéron, P. (2005), *Réduction de traînée aérodynamique par contrôle passif des écoulements-analyse par PIV*. In Colloque de visualisation et de traitement d'images en mécanique des fluides (FLUVISU 11), EC Lyon, France.
13. Fekaouni, M.F., Fekaouni, M. Maspeyrot, P. (2014) *Contrôle de l'écoulement d'air autour d'un modèle réduit d'un véhicule attelant une remorque*, Int. Conf. Modeling and Simulation 2014, Blida, Algérie, 2014.
14. Franck, G., D'Elía, J. (2004), *CFD modeling of the flow around the Ahmed vehicle model*. CIMEC INTEC (UNL-CONICET), PTLC, Santa Fe, Argentina.
15. Gilliéron P. (2002), *Contrôle des écoulements appliqué à l' automobile. État de l'art*, Mécanique & Industries 3(6), 515-524. doi: 10.1016/S1296-2139(02)01197-1
16. Cousteix, J. (1989), Aérodynamique, Turbulence et Couche Limite, Cépaduès éditions, ISBN 2854282108
17. Arnal, D., Cousteix J., Michel R. (1976), *Boundary layer developing with positive pressure gradient in an external turbulent flow*, La Recherche Aérospatiale, n°1976-1.
18. Granville, P.S. (1985), *Mixing-length formulations for turbulent boundary layers over arbitrarily rough surfaces*, J Ship Res. 29(4): 223-233.
19. Onorato, M., Costelli, A.F., Garonne, A. (1984), *Drag measurement through wake analysis*, in: SAE, SP-569, Int. Congress and Exposition, Detroit, MI, 1984, pp.85-93.
20. Gilliéron, P., Kourta, A. (2013), Aérodynamique automobile pour l'environnement, le design et la sécurité, 2e édition, Cépaduès éditions, p.340. ISBN-10: 236493091X